Equilibrium and mid-infrared driven vibrational dynamics of artificial hydrogen-bonded networks

Jaane Seehusen,[a] Dirk Schwarzer,[b] Jörg Lindner[a] and Peter Vöhringer*[a]

Stereo-selectively synthesized 1,3-poly-alcohols are introduced as low-dimensional spectroscopic model systems for molecular dynamics in hydrogen-bonded networks. The molecular and vibrational structures of the artificial networks are studied by means of density functional theory. The flexibility of the networks and the time scales associated with hydrogen-bond breakage and formation are investigated through Langevin dynamics simulations. Experimentally, the dynamics of the polyols are explored by femtosecond mid-infrared spectroscopy in the OH-stretching spectral region. Polyols with their hydroxyl groups distributed along the hydrocarbon backbone in an *all-syn* configuration are highly rigid and form an extended quasi 1-dimensional hydrogen-bond wire that is stable for tens of picoseconds. The mid-infrared pump–probe data on these rigid networks exhibit biexponential kinetics. This finding supports a mechanism for vibrational energy relaxation in *all-syn* polyols that is mediated by hydrogen-bond dissociation within 850 fs. The hydrogen-bond wire is subsequently re-established on a time scale of about 14 ps. In contrast, poly-alcohols with their OH groups in an *all-anti* configuration are highly flexible and display hydrogen-bond breakage–formation on a 100 fs time scale already at thermal equilibrium. As a result the pump–probe data are mono-exponential and can be understood in terms of pure intramolecular vibrational relaxation occurring with a time constant of 1.3 ps.

I. Introduction

Hydrogen-bonding is one of the most important non-covalent interactions in nature and can take place at the intermolecular as well as the intramolecular level.[1–3] For example, intermolecular hydrogen-bonding plays a crucial role in determining the physico-chemical properties of associated liquids.[4] The well-known anomalies of water that become apparent in a wide variety of its thermodynamic and transport properties can be traced back to the formation of a unique network of hydrogen-bonds that is highly random in both space and time. Furthermore, intermolecular hydrogen-bonding is very often involved in molecular recognition phenomena. In nature, it can lead to highly complex supramolecular architectures, the most famous examples of which are the helical duplex assemblies of nucleic acids carrying the genetic code of every individual biological organism.

At the intramolecular level, hydrogen-bonding becomes important in nature in determining the secondary and tertiary structure as well as the finite temperature dynamics of peptides and proteins. The function of proteins relies critically on the interplay of intramolecular and intermolecular hydrogen-bonding, the former being responsible for the creation of the suitable protein structure that is capable of spatially accommodating a given substrate and the latter being in charge of recognizing and binding the substrate reversibly.[5]

Because of its tremendous importance, hydrogen-bonding has been one of the primary targets of condensed phase physico-chemical research for a long time. Recently, time-resolved spectroscopy has become a particularly useful tool in disclosing highly detailed information regarding the vibrational dynamics in hydrogen-bonded systems.[6–11] To this end, an ultrashort pump-pulse resonantly excites a vibration that is coupled to the hydrogen-bonds of interest to the system. A variably delayed probe pulse is then used to interrogate the resultant vibrational population dynamics either through the recovery of the ground state bleach or the anharmonically-shifted absorption of the excited state.

It turns out that the stretching vibrations of hydroxyl (OH) or amine (NH) groups are particularly sensitive reporter modes of the structural details of the environment in which they are embedded.[12,13] In particular, it was shown both experimentally[14] and computationally[15–17] that in water the OH-stretching frequency decreases with a decreasing average nearest-neighbor O–O distance. Qualitatively speaking, a high-frequency hydroxyl oscillator is engaged in weak hydrogen-bonds whereas an OH-vibrator with a low frequency is typically involved in strong hydrogen-bonds.

As a consequence hydrogen-bond fluctuations and, more dramatically, hydrogen-bond rupture and formation lead to the phenomena of vibrational dephasing and vibrational spectral diffusion. Such phenomena have been explored in great detail through IR photon echoes and two-dimensional fs-IR spectroscopies by the groups of Miller and Elsaesser[18]

[a] *Lehrstuhl für Molekulare Physikalische Chemie, Institut für Physikalische und Theoretische Chemie, Rheinische Friedrich-Wilhelms-Universität, Wegelerstraße 12, 53115 Bonn, Germany. E-mail: p.voehringer@uni-bonn.de*
[b] *AG Reaktionsdynamik, Max-Planck-Institut für biophysikalische Chemie, Am Faßberg 11, 37077 Göttingen, Germany*

for the case of neat liquid H_2O as well as by the groups of Tokmakoff[17,19,20] and Fayer[21,22] for the isotopomeric systems of HOD in H_2O and HOD in D_2O, respectively.

To unambiguously disentangle the correlation between energy relaxation on one hand and hydrogen-bond geometry on the other, we have recently performed systematic fs-mid-IR experiments on water under various thermodynamic conditions ranging from the dilute supercritical phase to the dense liquid phase.[23,24] At sufficiently high temperatures, the spectroscopically observable kinetics were single-exponential in nature while at low temperatures and high densities (e.g. also under ambient conditions) the kinetics were found to be multi-exponential. We could demonstrate that in the first case vibrational spectral diffusion due to H-bond breakage and formation and vibrational energy relaxation are temporally well separated while in the second case both dynamics occur on very similar time scales. By extrapolation from an extensive set of rate coefficients that were experimentally determined at sufficiently high temperatures (i.e. when H-bond induced spectral diffusion is much faster than vibrational relaxation), a lifetime of the OH-stretching vibration under ambient conditions was derived that should be understood as an ensemble-averaged vibrational lifetime.

This paper intends to introduce stereo-selectively synthesized poly-alcohols as model systems for the vibrational spectroscopy and the molecular dynamics of hydrogen-bonded networks.[25,26] It will be shown that the stereochemical configuration of the OH-groups attached to the hydrocarbon backbone of the poly-alcohols influences the rigidity of the hydrogen-bond network and, therefore, determines the time scale of H-bond structural dynamics relative to that of vibrational energy relaxation. When favorably oriented, the hydroxyls can form an extended quasi-1-dimensional hydrogen-bond wire that is stable in liquid solution at room temperature over tens of picoseconds. In this case, the vibrational dynamics of the artificial network resembles very much that of hydrogen-bonded aggregates of lower alcohols dissolved in non-polar solutions or hydrogen-bonded networks in solid matrices.[27,28] In the opposite case of an unfavorable stereochemical configuration of the hydroxyls, hydrogen-bond wires may still form; they are however susceptible to ultrafast breakage and restructuring on time scales much faster than the initial infrared excitation. In this case, the vibrational dynamics of the artificial network are much more reminiscent of bulk hydrogen-bonded liquids at elevated temperatures.[23,24,29]

The paper is organized as follows. In the next section, some technical details related to our combined computational and experimental approach are described. Section III presents results from density functional theory on the molecular structure and the nature of the vibrations of the artificial hydrogen-bonded networks. We also present first results from Langevin molecular dynamics simulations to computationally explore the time scales of hydrogen-bond fluctuations. The next section summarizes our data obtained by stationary and femtosecond time-resolved spectroscopy in the OH-stretching spectral region of the networks. These will then be discussed in terms of a kinetic model that takes into account a dissociation of the hydrogen-bonds, i.e. their rupture induced by the initial mid-infrared laser excitation.

II. Methods

The low-dimensional hydrogen-bonded networks consisted of diastereo-selectively synthesized 1,3-poly-alcohols, whose molecular structure is schematically shown in Fig. 1. Their synthesis is based on an iterative aldol-condensation recently developed by Paterson and co-workers.[25,26,30,31] Following their protocols we have managed to prepare the diols ($n = 2$), tetrols ($n = 4$), and hexols ($n = 6$) of both the all-syn and the all-anti configuration. We have performed complementary studies on the diols and the hexols and their results support the major conclusions drawn in this paper. For space reason we will focus here on the tetrols only and postpone a presentation of the results obtained for the diols and the hexols to a future publication.

The methyl groups attached to the saturated hydrocarbon chain are directed into an all-anti configuration. The repulsive steric interactions between these bulky substituents are intended to hold the hydrocarbon backbone in an extended chain conformation similar to syndiotactic polypropylenes.[25] This in turn facilitates the formation of an extended hydrogen-bond network provided the hydroxyl groups are favorably oriented. Whereas this network formation can already be envisioned by intuition for the all-syn diastereomer of Fig. 1, one can predict that hydrogen-bonding in the all-anti counterparts is strongly inhibited by the methyl repulsion. Therefore, one can expect an entirely different hydrogen-bonded network both in terms of structure and also in terms of its dynamics. Samples were prepared by dissolving 7×10^{-4} mol dm^{-3} of the polyols in deuterated chloroform ($CDCl_3$). The solutions were kept in optical cells with CaF_2 windows and an optical path length of 2 mm suitable for stationary and time-resolved mid-infrared spectroscopy.

The molecular structures, the vibrational modes as well as the molecular dynamics of the polyols were investigated by means of extensive classical and quantum chemical calculations. Since the molecular size of these systems is rather large, it is quite time-consuming to discover the global optimized structure even for highly efficient state-of-the-art density functional theory (DFT). Therefore, a molecular mechanics conformational search along all torsional degrees of freedom of the hydrocarbon backbone was carried out using the AMBER force field[32] included in the Hyperchem package.

AMBER was also used for Langevin molecular dynamics[33] simulations in an effort to characterize the flexibility of the
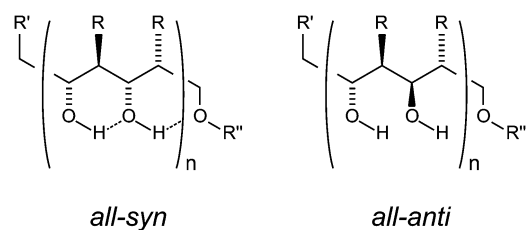

Fig. 1 Chemical structure of the poly-alcohols providing hydrogen-bonded networks of low-dimensionality. Left: all-syn-polyols, right: all-anti-polyols. The substituents R and R' are methyl groups while R″ = Bz corresponds to a benzyl group.

polyols and their hydrogen-bonded networks at room temperature in the presence of a liquid solvent. The velocity Verlet-algorithm[33] was used to integrate the Langevin equations of motion with a time step of 1 fs and a friction coefficient of 10 ps^{-1} as derived from the solvent self-diffusion coefficient.[34] During equilibration of the AMBER-optimized structures, velocities were rescaled at each time step thereby coupling the system to a constant temperature (300 K) external heat bath with a relaxation time of 100 fs.

The ten energetically lowest minima identified by the conformational search were further geometrically relaxed with the semi-empirical PM3-method.[35] These pre-optimized structures were then refined by means of DFT calculations. All DFT and semi-empirical calculations were performed with the ORCA program package developed by Neese.[36,37] The efficiency of the DFT part was enhanced at no significant loss of accuracy by invoking the resolution-of-identity (RI) approximation.[38] Since this approach necessitates a non-hybrid functional, we have chosen the Becke–Perdew functional, BP86.[39,40] The Ahlrichs' triple-ζ valence basis set, TZVPP, with three sets of polarization functions on all atoms was applied.[41] In addition, the RI-approximation needs an auxiliary Coulomb fitting basis (TZV/J) for the triple-ζ valence basis set, which was taken from the TURBOMOLE library.[42] Structure optimizations with and without geometrical constraints were performed in redundant internal coordinates using analytical gradients, whose double-sided numerical differentiation yielded harmonic vibrational frequencies. Following the suggestions by Neugebauer and Hess for computations at the RI-DFT/TZVPP level of theory, a correction factor of 1.005 for conversion from harmonic to fundamental vibrational frequencies was used.[43]

Femtosecond-mid-IR experiments were conducted with a pump–probe setup whose details were previously reported.[29] Briefly, a chirped-pulse regenerative amplifier delivering 170 fs duration pulses at a repetition rate of 1 kHz with energies as high as 800 μJ is used to synchronously drive two independently tunable optical parametric amplifiers (OPA), each of which is equipped with difference frequency generators (DFG) based on AgGaS$_2$. One of the OPA–DFG units is used as the pump source while the other one serves as the probe source.

Pump and probe pulses were sent through individual computer controlled optical delay lines and could be attenuated with a combination of half-wave plate and polarizer. Their relative polarization was set to the magic angle (54.7°) to suppress signal contributions originating from molecular reorientation. In addition, a reference beam was derived from a 50% beamsplitter through which the probe beam was sent. Pump and probe pulses were spatially overlapped inside the sample using a 45° off-axis parabolic Au-mirrors with an effective focal length of 10 cm. An identical mirror was used to re-collimate the beams emerging from the sample. Probe and reference pulses were then imaged onto the entrance slits of a 0.2 m monochromator whose exit plane was equipped with a 2 × 32 pixel HgCdTe-array detector for referenced frequency-resolved detection of the pump-pulse induced optical density of the sample.

III. Results

Quantum-chemical and molecular dynamics calculations

Fig. 2 and 3 summarize the molecular structures corresponding to the lowest energy minima of the *all-syn* and *all-anti* tetrols using the computational strategy outlined above.

Focussing first on the *all-syn* diastereomer we recognize that an extended hydrogen-bonded network is formed in accordance with the predictions of ref. 25. This network formation is indeed facilitated by the cooperative effects of steric repulsion between the methyls and the favorable alignment of the hydroxyls thereby forcing the hydrocarbon backbone to adopt a unique conformation.

The network within the molecule is rather homogeneous with hydrogen-bond lengths that merely vary between 1.76 and 1.78 Å. The only exception is the hydrogen bridge between the ether oxygen and its neighboring hydroxylic proton, which is considerably weaker and with a length of 1.85 Å substantially stretched in comparison to the pure inter-hydroxylic hydrogen-bonds. Likewise, the O–O distance between adjacent hydroxyls varies only between 2.61 and 2.65 Å for the contacts of the type O–H $\cdots$ O–H and is somewhat longer (2.71 Å) for the weaker O–H $\cdots$ O–Bz interaction.
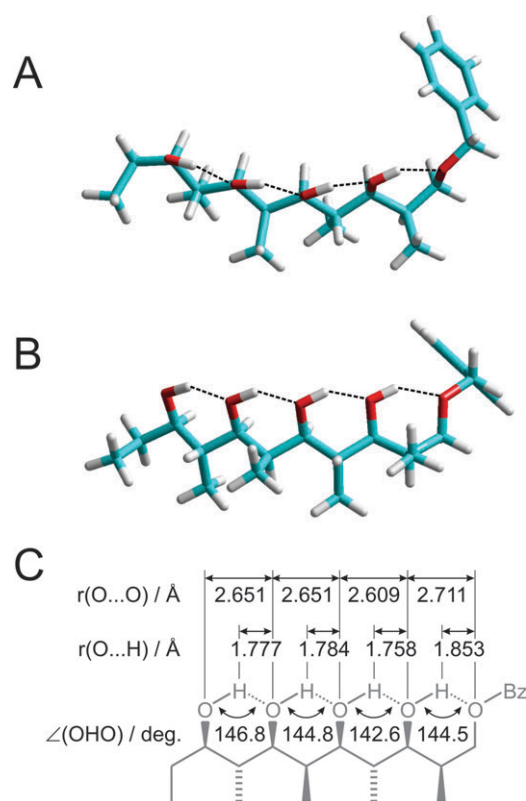

Fig. 2 Optimized structure of the *all-syn* tetrol. (A) Top view of the hydrocarbon backbone emphasizing the almost perfect parallel alignment of the hydroxyl groups and the quasi-linear nature of the hydrogen-bonded network. (B) Side view of the hydrocarbon backbone emphasizing the *all-syn* configuration of the OH groups and the simultaneous *all-anti* configuration of the methyl substituents. (C) Summary of the structural parameters including hydrogen-bond length, hydrogen-bond angle, and distance between adjacent oxygens.
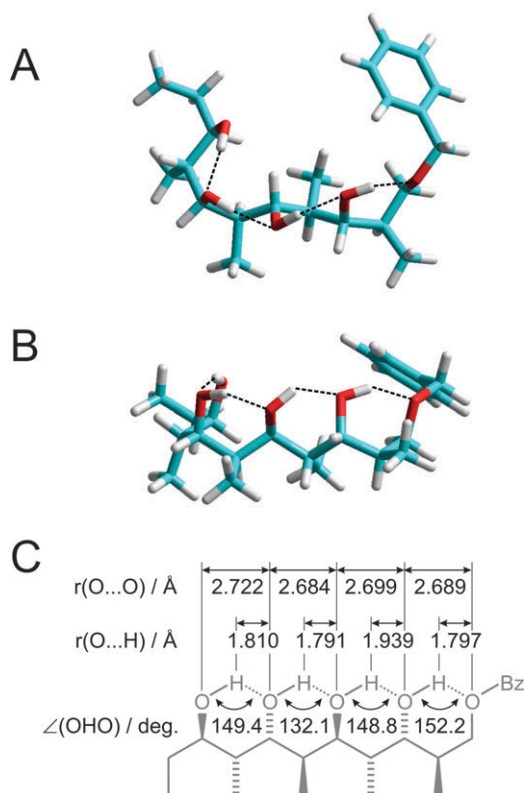
Fig. 4 Vibrational structure (sticks) and spectra (curves) from DFT calculation of the optimized geometries shown in Fig. 2 and 3. Top: *all-syn* tetrol, bottom: *all-anti* tetrol. The spectra were calculated from the stick spectra by convolution with a Lorentzian line shape exhibiting a full width at half maximum of 20 cm^{-1}.

Fig. 3 Optimized geometry of the *all-anti* tetrol. (A) Top view of the hydrocarbon backbone emphasizing its curled structure, the misalignment of the hydroxyl groups, and the resulting highly strained nature of the hydrogen-bonded network. (B) Side view of the hydrocarbon backbone. (C) Summary of the structural parameters including hydrogen-bond length, hydrogen-bond angle, and distance between adjacent oxygens.

The almost perfect spatial alignment of the OH-groups is also highlighted by the hydrogen-bond angles all equaling (145 ± 2) degrees and by a very large overall molecular dipole moment of 9.6 Debye. The latter quantity can be understood in terms of a bond dipole model, *i.e.* by the additivity of the four individual hydroxyl bond dipoles all pointing nearly along the same axis. Inspection of the structure from atop (Fig. 2A) reveals a slight curvature of the hydrogen-bond wire, which might indicate some minor strain on the hydrocarbon backbone due to a small residual repulsion between the next-nearest methyl groups, *i.e.* between those CH$_3$-groups that are attached to the main alkyl chain with the same stereochemical configuration.

As opposed to the *all-syn* diastereomer, the refined structure of the *all-anti* tetrol is highly surprising (*cf.* Fig. 3). It lies about 2220 cm^{-1} above the optimized structure of the *all-syn* diastereomer and contrary to the initial expectations, it does exhibit an extended hydrogen-bonded network. The formation of this network is made possible by the adoption of a pronounced coiled conformation by the hydrocarbon backbone thereby avoiding the strongly repulsive contacts between the methyls while at the same time allowing for hydrogen-bonding between the improperly configured hydroxyl groups.

The network is not as regular as in the *all-syn* species with hydrogen-bond lengths distributed between 1.79 and 1.94 Å.
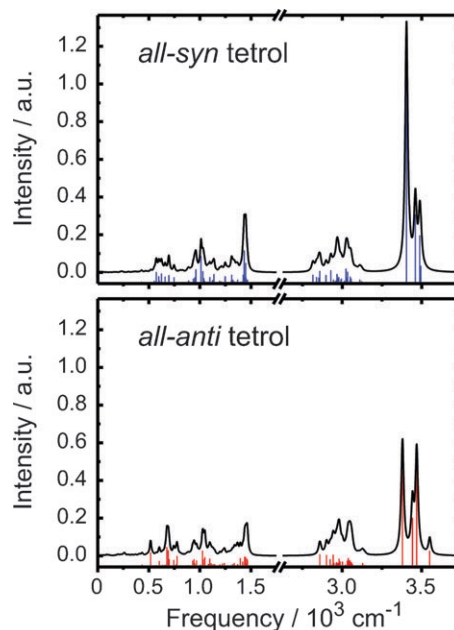
Likewise, the distances between adjacent oxygens are much larger as compared to the *all-syn*-diastereomer and scatter between 2.69 and 2.72 Å. Finally, a wide spread of hydrogen-bond angles ranging from 132 to 152° together with a significantly smaller overall dipole moment of only 5.75 Debye emphasizes the spatially irregular nature of the hydrogen-bonded network.

A vibrational analysis was carried out on the refined structures of the *all-syn* and *all-anti* tetrol at the RI-DFT/TZVPP level of theory. The calculated infrared spectra of the two compounds are reproduced in Fig. 4. For both systems, the vibrational structure can be divided into three different regions. From 3300 to 3600 cm^{-1}, the spectra are dominated by the hydroxyl-stretching vibrations. The CH-stretching region lies between 2700 and 3200 cm^{-1}. In the region from 1250 to 1700 cm^{-1}, the CH- and OH-bending modes can be found. Finally, below 1000 cm^{-1}, one can identify the low-frequency modes (lfm) of the hydrocarbon backbone. Despite the qualitatively similar vibrational structure of the two diastereomeric forms, there are subtle differences in particular in the OH-stretching region, which should be pointed out.

There are four OH-stretching normal modes for each diastereomer. In the *all-syn* diastereomer, these can be understood as linear combinations of the four OH local modes, *i.e.* the modes are spatially fully delocalized over the hydrogen-bonded network. Because of the structural regularity of the hydrogen-bonded network, the OH-stretching resonances of the *all-syn* compound can be found in a rather narrow frequency interval ranging from 3404 to 3494 cm^{-1}.

The resonance with the highest intensity corresponds to a OH-normal mode, in which all four OH-oscillators vibrate collectively in phase. Illustrating the delocalized hydroxyl

displacements of the OH-stretching vibrations by a standing wave across the hydrogen-bonded network, this mode does not exhibit any node pattern. It is found at a frequency of 3404 cm^{-1}, *i.e.* strongly red-shifted by about 300 cm^{-1} in comparison to the OH-stretching frequency of alcohols carrying a single OH-oscillator only. For example, the same DFT-methodology locates the OH-stretch of methanol at 3719 cm^{-1} whereas high-resolution infrared spectroscopy identifies the methanol OH-stretching fundamental at 3686 cm^{-1}.[44]

The OH-stretching vibration with the highest frequency is a delocalized mode in which adjacent hydroxyls oscillate out of phase. The standing wave representing the OH-displacements across the hydrogen-bonded network exhibits three nodes for this mode. It is found at 3494 cm^{-1} and in the presence of finite line broadening (see curves in Fig. 4), it merges into a single resonance with a delocalized mode exhibiting two nodes and having a fundamental frequency of 3488 cm^{-1}. Finally, a fourth mode whose standing wave representation possesses a single node lies at an intermediate frequency of 3459 cm^{-1}.

In contrast to the *all-syn* form, the four OH-stretching resonances of the *all-anti* diastereomer are distributed over a wider frequency range because of the geometrically more heterogeneous distribution of its hydrogen-bonded contacts (*cf*. Fig. 2 and 3). The OH stretching modes of the *all-anti* tetrol are of fundamentally different nature. This is because of the dramatically different hydrogen-bond geometries along the network which strongly perturbs the collectivity of the OH motions. Particularly pronounced is the difference between the hydrogen-bond angles and lengths of the two central hydrogen-bridges (132 *versus* 148° and 1.79 *versus* 1.94 Å, respectively; see Fig. 4).

These disparate geometries lead to two OH-stretching vibrations that are of true local mode character. One mode has a frequency of 3550 cm^{-1} and corresponds to the OH-stretch of the hydroxyl group donating a hydrogen-bond to the benzyl ether oxygen. Its neighboring hydroxyl group represents the site of another local mode oscillating at a frequency of 3469 cm^{-1}. The two remaining OH-stretching modes are shared between the other two hydroxyls and can be viewed as their in-phase and out-of-phase collective stretching motions. They exhibit frequencies of 3379 and 3442 cm^{-1}.

The rigidity of the backbone and of the hydrogen-bonded networks in the presence of a non-polar environment at room temperature was further explored by Langevin molecular dynamics simulations using the AMBER force field for the intramolecular interactions.[32,33] Representative trajectories of the four hydrogen-bond lengths are shown in Fig. 5 for each diastereomer over a time period of 50 ps.

It is obvious that the absolute magnitude of the bond length fluctuations is much smaller for the *all-syn* tetrol as compared to its *all-anti* counterpart. This holds true for all four potential hydrogen-bonded contacts. In the *all-syn* case, a hydrogen-bond breakage event can be identified only once at about 11 ps and only for the contact to the benzyl ether (H-bond # 1) when this bond length increases by roughly 1.5 Å. However, this bond reforms very quickly after ~1 ps. All other contacts remain intact and fluctuate about their equilibrium position with a standard deviation of 0.1 Å for the entire duration of
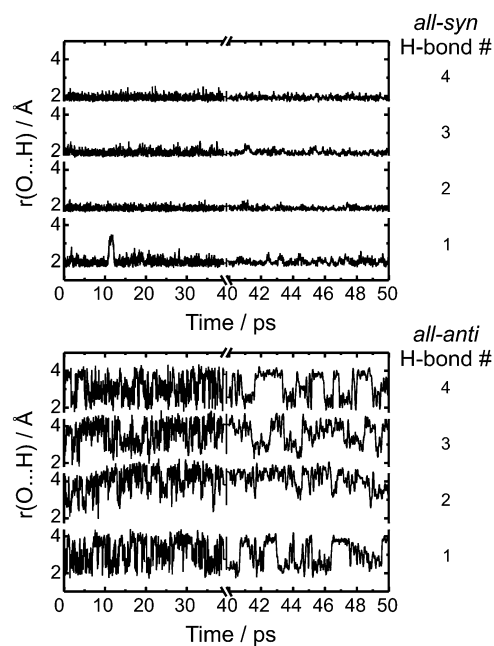

Fig. 5 Lengths of the four hydrogen-bridges for the *all-syn* tetrol (top) and the *all-anti* tetrol (bottom) along a 50 ps trajectory from Langevin molecular dynamics simulations. Note the break of the time axis at 40 ps emphasizing the bond length fluctuations reminiscent of hydrogen-bond breakage and formation more clearly on shorter time scales (*e.g.* for 40 to 50 ps).

the trajectory. From the trajectory, one can also reconstruct the distribution of hydrogen-bond lengths as shown in Fig. 6 (left). These quantities are well behaved and display a unique maximum corresponding to a unique stable molecular geometry around which the molecule undergoes small-scale thermal fluctuations.
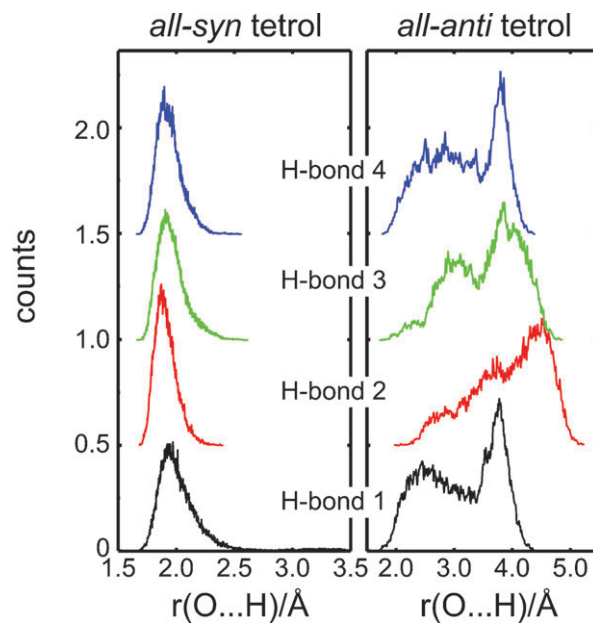

Fig. 6 Distribution of bond lengths of the four hydrogen-bridges for the *all-syn* tetrol (left) and the *all-anti* tetrol (right) derived from the 50 ps trajectory shown in Fig. 5.

8488 | *Phys. Chem. Chem. Phys.*, 2009, **11**, 8484–8495

This journal is © the Owner Societies 2009

The stochastic hydrogen-bond length excursions of the *all-anti* diastereomer are dramatically different both in terms of the absolute magnitude and in terms of the frequency of bond fission events (see Fig. 5, bottom). One can observe an intermittent breaking and forming of hydrogen-bonds on all four hydroxyl sites. A more detailed analysis of the underlying dynamics will follow. At this stage, it suffices to derive the distribution of hydrogen-bond lengths for the *all-anti* tetrol, which is reproduced in Fig. 6 (right).

These distributions are much broader as compared to the *all-syn* diastereomer and perhaps with the exception of hydrogen-bond number 2 exhibit at least two maxima. Obviously, at thermal excitations there are significantly more structures accessible to the molecule than only one. These can interconvert on time scales much shorter than 1 ps.

These findings are in complete agreement with the observation by Paterson and co-workers and also by us that the *all-syn* tetrol features four distinct ^{1}H-NMR resonances originating from the hydroxylic protons.[25] This indicates that the intra-molecular hydrogen-bond network indeed assumes a unique structure in which each hydroxylic proton experiences a slightly different molecular environment and, hence, a slightly different NMR chemical shift. Interconversions to other stable structures that would lead to line broadening of the four magnetic resonances or even to their coalescence are apparently slow on the NMR time scale.

This is in stark contrast to the *all-anti* tetrol which features only a single broad NMR resonance from its hydroxylic protons indicating that chemical exchange is fast on the NMR time scale.[25] In light of the Langevin dynamics reported here, this finding is not at all surprising.

Stationary and time-resolved mid-IR spectroscopy

The linear Fourier-transform infrared spectra (FTIR) of the two diastereomeric tetrols in liquid $CDCl_3$ solution are reproduced in Fig. 7. It is important to note that both compounds have a strong tendency for dimerization in non-polar solvents. Hence, all experiments reported herein have been carried out with solute concentrations below 7×10^{-3} mol dm^{-3} at which dimer formation becomes negligible as evidenced by dilution series of FTIR spectra.

The *all-syn* tetrol shows an OH-stretching band that peaks at 3388 cm^{-1} and has an enormous full spectral width at half
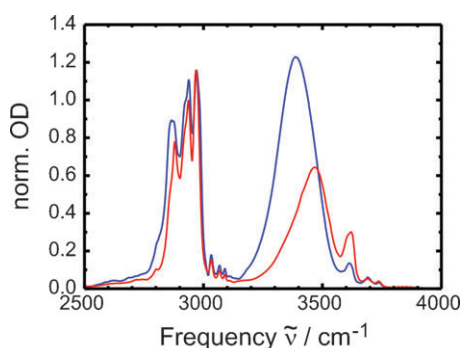

Fig. 7 Linear Fourier-transform infrared spectra in the OH- and CH-stretching region of the *all-syn* (blue) and *all-anti* (red) tetrol dissolved in deuterated chloroform.

maximum (FWHM) of 183 cm^{-1}. A smaller blue-shifted band centered at 3614 cm^{-1} resembles the symmetric stretching mode of monomeric water molecules in $CDCl_3$ and can therefore be assigned to a very few dangling OH-bonds of the tetrol primarily interacting with the non-polar solvent. Additional even smaller bands at higher frequencies correspond to overtone and combination transitions. The major band around 3388 cm^{-1} is without doubt due to hydrogen-bonded hydroxyls. For comparison, the OH-stretching resonance of HOD in D_2O[14] at 296 K and 1 bar, which has a width of roughly 230 cm^{-1}, is centered at 3403 cm^{-1}, *i.e.* very close to the band center of the *all-syn* tetrol, whose OH-stretching modes were found to be delocalized over the network.

The FTIR spectrum of the *all-anti* species is markedly different. The OH-band located at 3605 cm^{-1}, which is indicative of dangling hydroxyl groups, has gained intensity relative to the complementary band of the *all-syn* tetrol. In parallel, the major band has lost intensity and is substantially blue shifted as compared to its *all-syn* counterpart. It is now centered at 3467 cm^{-1} but still has a very large spectral width of 169 cm^{-1} (FWHM).

These findings clearly indicate that the hydrogen-bonds are much weaker when the OH-groups adopt an *all-anti* configuration and that on average the hydrogen-bonded network must be considerably disrupted as demonstrated by the increased absorption of the "free" OH-band at the expense of the "bound" OH-band. It is quite interesting to note that the band shapes of the "bound" OH-resonance are also very different for the two diastereomers. Whereas the absorption profile of the *all-syn* tetrol is rather symmetric and almost Gaussian with respect to the band center, it appears highly asymmetric in the spectrum of the *all-anti* tetrol with a pronounced high-frequency tail. This might suggest that the underlying line broadening mechanisms are entirely different for the two species. Some computational support in favor of such an interpretation may be available from the molecular dynamics simulations discussed above. We are currently following up on this hypothesis experimentally by means of two-dimensional femtosecond infrared spectroscopy.

Here, we wish to report on conventional time-resolved fs-mid-IR-spectroscopy. Fig. 8 reproduces transient differential absorbance spectra of the *all-syn* tetrol in $CDCl_3$ solution. In these experiments, the spectrum of the pump-pulses (dashed curve) covered the entire linear OH-stretching absorption of this species. At short delays after excitation, one can observe the expected signal contributions: (i) the bleaching of the vibrational ground state and the stimulated emission from the OH-stretching excited state and (ii) the anharmonically-shifted transient absorption of the excited state. Both signals decay in concert on a picosecond time scale. However, they do so without forming an isosbestic point. Rather, a considerable time-dependent red-shift of the bleaching–emission signal is clearly discernible.

To emphasize this complex spectro-temporal response more clearly, a few representative time traces at various probing frequencies are reproduced in Fig. 9. Whereas a transient recorded in the absorptive region of the OH-stretching excited state (*i.e.* at 3185 cm^{-1}) decays single-exponentially with a
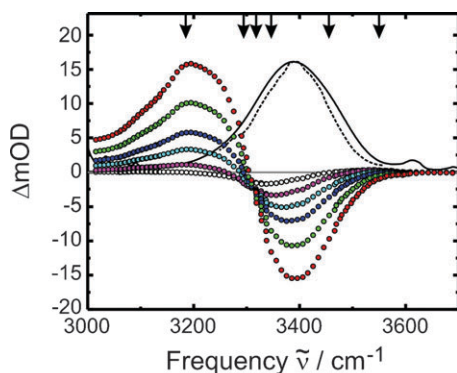
Fig. 8 Transient differential absorbance spectra of the *all-syn* tetrol at pump–probe time delays of 600 fs (red), 1 ps (green), 1.5 ps (blue), 2 ps (cyan), 3 ps (magenta), and 10 ps (white). The solid curve corresponds to the linear FTIR-spectrum of the compound while the dashed curve is the spectrum of the pump-pulses.

Fig. 10 Transient differential absorbance spectra of the *all-anti* tetrol at pump–probe time delays of 600 fs (red), 1 ps (green), 1.5 ps (blue), 2 ps (cyan), 3 ps (magenta), and 10 ps (white). The solid curve corresponds to the linear FTIR-spectrum of the compound while the dashed curve is the spectrum of the pump-pulses.
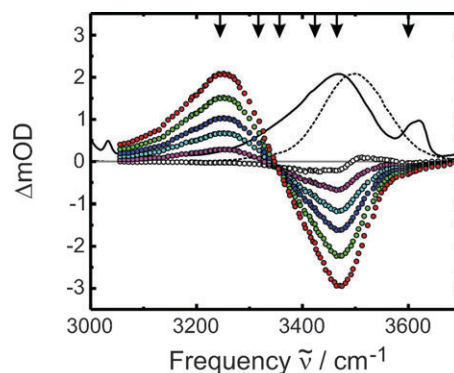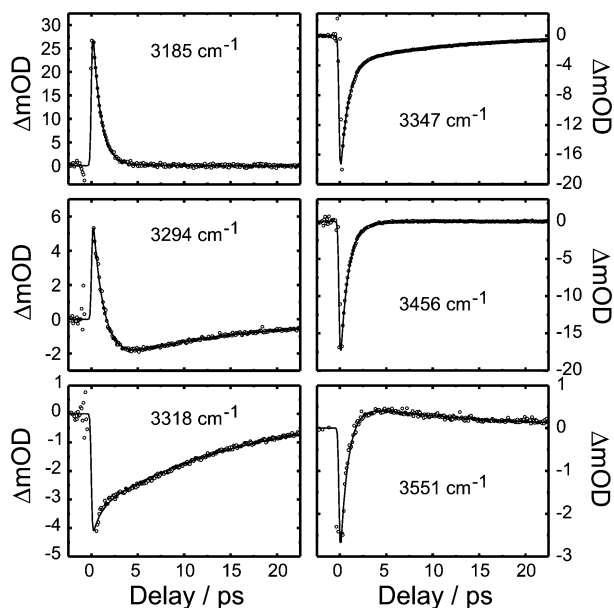

Fig. 9 Time-resolved transient differential transmission data for the *all-syn* tetrol in CDCl$_3$ recorded with various probe frequencies distributed across the OH-stretching spectral region as indicated by the arrows in Fig. 8. The solid curves correspond to the model simulation described in Section IV.

constant identical to that of the decay of the excited-state absorption, namely 0.85 ps. Finally, on the far blue edge of the linear absorption spectrum, the signals are again very complex, now being initially emissive at short delays below 1 ps and absorptive for longer delays.

Transient differential absorbance spectra of the *all-anti* tetrol are reproduced in Fig. 10. Qualitatively, the spectra are similar to those of the *all-syn* diastereomer with a negative ΔOD in the blue spectral region due to bleaching of the ground vibrational state and stimulated emission from the vibrationally excited state. In the red spectral region, one can again identify the anharmonically-shifted transient absorption from the excited OH-stretching state.
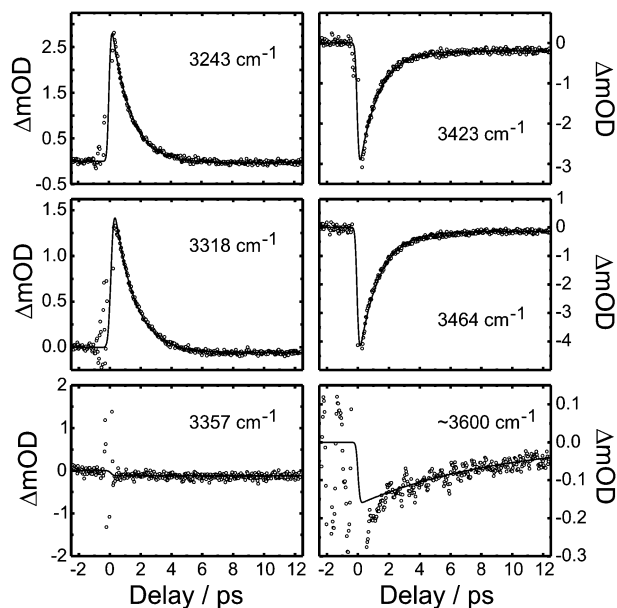
time constant of 0.85 ps, the nature of the temporal traces near the cross-over region around 3294 cm^{-1} changes from being absorptive within the first picosecond to emissive for longer delays.

With a slightly higher probing frequency of 3318 cm^{-1} the signal contains only bleaching–emission contributions which do not decay completely even after 20 ps. Fitting a single-exponential to this signal reveals a time constant of 14 ps. For frequencies up to the maximum of the linear absorption, the signals are purely emissive and decay bi-exponentially with time constants of 0.9 ps and 16 ps.

When probing is performed with frequencies slightly tuned to the blue of the OH-band maximum (*e.g.* at 3456 cm^{-1}), the bleach recovers in a single-exponential fashion with a time

Fig. 11 Time-resolved transient differential transmission data for the *all-anti* tetrol in CDCl$_3$ recorded with various probe frequencies distributed across the OH-stretching spectral region as indicated by the arrows in Fig. 9. The solid curves correspond to the model simulation. Notice that around time zero and at negative delays the signals are distorted by coherent coupling effects of the pump and probe pulses.

Yet, there is also a marked difference between the pump–probe spectra of the two diastereomeric tetrols. Whereas in the *all-syn* polyol an apparent time-dependent red-shift of the bleaching signal was observed (see Fig. 8), such a feature is entirely absent for the *all-anti* tetrol. As a result, the spectra of the latter compound form a characteristic isosbestic point at a probe-frequency of 3357 cm^{-1} (see Fig. 10).

Again, a few representative time-resolved pump–probe traces are shown in Fig. 11 to illustrate the OH-stretching vibrational kinetics of the *all-anti* tetrol. For frequencies lower than the isosbestic frequency, the transient absorption decay is single-exponential with a time constant of 1.3 ps. Likewise, the bleach–emission decay to the blue of the isosbestic point occurs also with a time constant of 1.3 ps. Exactly at the isosbestic probe-frequency, the signal is temporally invariant (as it should be) and only a very small constant background may be discernible within the signal-to-noise ratio. Finally, probing in the frequency range around the "free" OH-band yields very small signals only. When averaged over a frequency band ranging from 3580 to 3625 cm^{-1}, the kinetics are considerably slower as compared to lower probing frequencies and can be fitted by a single-exponential decay with a time constant of roughly 9 ps.

IV. Discussion

Firstly, the kinetic nature underlying the spectro-temporal response in the OH-stretching spectral region of the tetrols needs to be addressed. Vibrational energy relaxation (VER) of OH-stretching vibrations has been studied both in polar[45,46] and non-polar liquids.[47–49] For example, the lifetime of the first OH-stretching excited state of monomeric water in dilute acetonitrile solution has been determined to be 12 ps.[46] This stretching mode lifetime increases to about 90 ps when water is dissolved in a non-polar solution like deuterated chloroform.[47] Only in pure liquid water or in its isotopic mixtures is the lifetime of the OH-stretching mode shorter than 1 ps.[23,50–52]

For larger alcohols vibrational relaxation becomes considerably more complex as compared to the triatomic water system because of the large number of intramolecular pathways, which facilitate the resonant flow and partitioning of the initial OH-stretching quanta into combination and overtone excitations of other modes of the molecule.[53,54]

For monomeric alcohols dissolved in non-polar solvents the OH-stretching vibrational lifetime was found to be well in excess of 1 ps. For example, for ethanol highly diluted in carbon tetrachloride Laenen and Rauscher identified a lifetime of 8 ps.[55] They furthermore concluded that vibrational energy transfer (VET) to CCl_4 is of minor importance because of the energetic mismatch between the solute's OH-stretch and the solvent's low-frequency modes. Instead, the CH-stretching modes serve as the accepting modes for intramolecular energy flow since their combination quanta with CO-stretching and COH-bending modes are Fermi-resonant to the initially prepared OH-stretching excited state.[55]

As for water the lifetime decreases when the alcohols are brought into a hydrogen-bonding environment.[27,28] In particular, a very short lifetime was found for the lower alcohols, methanol to propanol, even in a non-polar solvent

when the concentration was sufficiently high to enable the formation of molecular aggregates. In this case, vibrational relaxation can be accompanied by breakage of the hydrogen-bond to which an excited OH-oscillator is coupled.[27,28] Such dissociation events become possible because the typical binding energy of the hydrogen bridge is lower than the photon energy delivered by the infrared pump pulse.[56] Woutersen *et al.* showed that mid-IR pump-induced dissociation in hydrogen-bonded ethanol aggregates can occur on a time scale faster than 1 ps.[27] The subsequent hydrogen-bridge re-formation was found to occur with a time constant of 15 ps.

Such hydrogen-bond ruptures certainly need to be taken into account when interpreting the pump–probe data on the *all-syn* tetrol. This is particularly important in light of the delocalized nature of the OH-stretching vibrations revealed by the DFT calculations. Hydrogen-bond breakage will cause the vibrational modes to localize on a particular OH-bond leading to a blue-shifted resonance as demonstrated by a comparison to the *all-anti* tetrol whose OH-modes have a more local character and a considerably higher resonance frequency.

The incident pump photon of 3400 cm^{-1} carries enough energy to break one of the hydrogen-bonded contacts. Hydrogen-bond breakage might also lead to redistribution of the photon energy over a larger set of vibrational modes of the molecule (intramolecular vibrational redistribution, IVR). IVR might even be complete so as to form a canonically excited "hot" molecule. In the case of complete IVR, one can crudely estimate the resultant temperature jump for the *all-syn* tetrol from the partition functions of its 188 oscillators. Using the harmonic frequencies determined from the DFT calculations such a simple calculation yields a temperature jump of 75 K for an excitation energy of 3400 cm^{-1}.

Finally, following H-bond rupture and IVR, the excess vibrational excitation will be dissipated into the surrounding solvent (vibrational energy transfer, VET)—a process which may be termed "cooling" provided the preceding IVR was complete. Obviously, the dependence of the vibrational spectrum on temperature also needs to be accounted for.

To simulate the data for the *all-syn* tetrol a kinetic model is adopted that was successfully used in the past to interpret the fs-mid-IR pump–probe data obtained for ethanol oligomers (see Fig. 12) in non-polar solvents.[27] The mid-IR excitation of the molecule in its vibrational ground state, $|0\rangle$, at time $t = 0$ is connected with the OH-stretching absorption cross section, σ_{01}. In addition to the ground state bleach, the pump pulse creates population in the first excited OH-stretching state, $|1\rangle$,
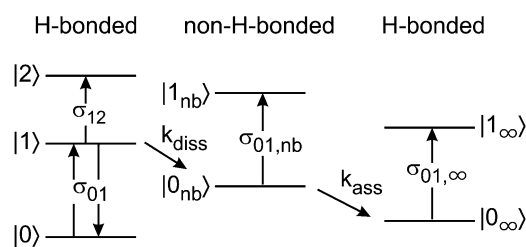

Fig. 12 Energy-level scheme (including hydrogen-bond dissociation, re-association and spectroscopic transitions) used for simulating the pump–probe data on the *all-syn* tetrol.

from which an anharmonically-shifted absorption can be observed with the cross section, σ_{12}. IVR and H-bond dissociation is kinetically described by the rate constant, k_{diss}, and converts $|1\rangle$ into the vibrational OH-stretching ground state, $|0_{\text{nb}}\rangle$, of the molecule with a disrupted hydrogen-bond network. Consequently, the OH-stretching vibrations are less collective in nature and their increased local mode character is expressed by an OH-stretching absorption cross section, $\sigma_{01,\text{nb}}$, that is substantially shifted to higher frequencies as compared to σ_{01}.

As mentioned above, the state, $|0_{\text{nb}}\rangle$, may or may not correspond to the "hot" molecule depending upon whether or not the incident pump photon energy is canonically distributed overall the vibrational modes of the tetrol. This can be clarified by comparing the difference absorption cross section $\sigma_{01,\text{nb}} - \sigma_{01}$ of this state with a thermal difference cross section obtained independently from temperature-dependent stationary FT-IR spectra of the tetrol (*vide infra*).

Finally, the *all-syn* tetrol is driven back to its equilibrium geometry thereby re-establishing its hydrogen-bond wire. At the same time, the initial photon energy will be dissipated into the surrounding solvent; *i.e.* the molecule effectively "cools" by VET. The H-bond association and "cooling" process is accounted for by the rate constant, k_{ass}, and leads to the OH-stretching ground state, $|0_{\infty}\rangle$, whose apparent absorption cross section at long pump–probe delays, $\sigma_{01,\infty}$, is permitted to slightly differ from that at thermal equilibrium due to the limited scan range of the pump–probe data.

The system of coupled kinetic rate equations representing the time-dependent populations in each of the vibrational states sketched in Fig. 12 can be solved analytically. With these solutions, one can express the pump-induced differential absorbance of the system as a function of the pump–probe time delay, t, and of the probe-frequency, $\tilde{\nu}$, according to

$$\Delta\text{OD}(t,\tilde{\nu}) = \frac{k_{\text{diss}}}{k_{\text{diss}} - k_{\text{ass}}}(\Delta\sigma_{\text{nb}} - \Delta\sigma_{\infty})\exp(-k_{\text{ass}}t)$$
$$+ \frac{k_{\text{diss}}(\Delta\sigma - \Delta\sigma_{\text{nb}}) - k_{\text{ass}}(\Delta\sigma - \Delta\sigma_{\infty})}{k_{\text{diss}} - k_{\text{ass}}}\exp(-k_{\text{diss}}t)$$
$$+ \Delta\sigma_{\infty}$$

$$(1)$$

where the probe-frequency-dependent difference cross sections, $\Delta\sigma_i = \Delta\sigma_i(\tilde{\nu})$, are given by

$$\Delta\sigma(\tilde{\nu}) = \sigma_{12}(\tilde{\nu}) - 2\sigma_{01}(\tilde{\nu}),$$
$$\Delta\sigma_{\text{nb}}(\tilde{\nu}) = \sigma_{01,\text{nb}}(\tilde{\nu}) - \sigma_{01}(\tilde{\nu}), \text{ and} \quad (2)$$
$$\Delta\sigma_{\infty}(\tilde{\nu}) = \sigma_{01,\infty}(\tilde{\nu}) - \sigma_{01}(\tilde{\nu}).$$

The pump–probe time traces at a given probe-frequency can be fitted by a double-exponential decay to which a constant background signal is added. By fitting all experimentally determined pump–probe time traces as a function of probe-frequency one obtains in principle two time constants, two amplitudes and a temporally invariant offset, all of which are probe-frequency dependent.

Our full data set on the *all-syn* tetrol consists of a total number of 101 time-resolved pump–probe transients

distributed over a probe-frequency interval from 3000 to 3700 cm^{-1}. At each probe-frequency, 300 data points were recorded to cover a delay range up to about 20 ps. To reduce the overall number of fitting parameters dramatically, the fitting procedure was instructed to use the two rate constants as global fitting parameters while optimizing the amplitudes as well as the offset locally for each probe-frequency. Thus and in contrast to the work of ref. 27, the two rate coefficients were viewed as frequency-independent quantities.

The dissociation rate constant was found to be $k_{\text{diss}} = 1/(0.85\text{ ps})$ while the association rate coefficient was $k_{\text{ass}} = 1/(14\text{ ps})$. The dissociation rate is obviously very high. This finding is however in good agreement with the earlier work on mid-IR-induced hydrogen-bond rupture in ethanol oligomers where its time constant was found to vary between 250 fs and 900 fs depending upon the excitation frequency.[27]

We are currently performing non-equilibrium molecular dynamics calculations on the *all-syn* compound with differently disrupted networks as initial configurations to further explore the time scale of hydrogen-bond re-association numerically and to test whether the assignment of the slower exponential is also reasonable. At this stage it suffices to note that Bakker and co-workers identified a very similar rate constant of $1/(15\text{ ps})$ for hydrogen-bond recombination of ethanol oligomers in CCl$_4$ solution.[27]

From the three probe-frequency-dependent amplitudes we can retrieve the three difference cross sections given in eqn (2). These quantities are reproduced in Fig. 13 and permit for a critical assessment of the model's validity. The corresponding fits are compared in Fig. 9 (solid curves) to the experimental pump–probe traces at representative probing frequencies. As can be seen all fits are in excellent agreement with the data.

Of particular interest is the difference cross section, $\Delta\sigma_{\text{nb}}(\tilde{\nu}) = \sigma_{\text{nb}}(\tilde{\nu}) - \sigma_{01}(\tilde{\nu})$, *i.e.* the difference of the absorption cross section of the tetrol with the hydrogen-bond network disrupted relative to the molecule with the network intact. As expected the perturbed species has an increased absorption at frequencies higher than the stationary absorption, *i.e.* the unperturbed molecule. Concurrently, a bleaching due to the disrupted network is seen to the red of the linear absorption.
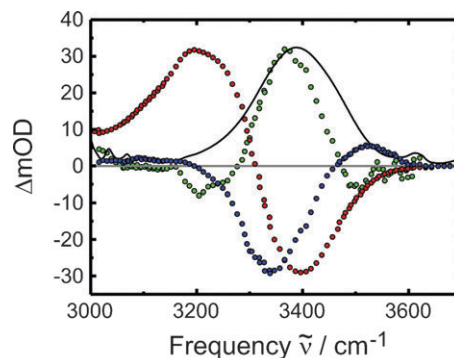

Fig. 13 Difference cross sections of the *all-syn* tetrol derived from the global fitting analysis of the pump–probe data. Red: $\Delta\sigma(\tilde{\nu}) = \sigma_{12}(\tilde{\nu}) - 2\sigma_{01}(\tilde{\nu})$, blue: $\Delta\sigma_{\text{nb}}(\tilde{\nu}) = \sigma_{01,\text{nb}}(\tilde{\nu}) = \sigma_{01,\text{nb}}(\tilde{\nu}) - \sigma_{01}(\tilde{\nu})$ multiplied by a factor of 9, green: $\Delta\sigma_{\infty}(\tilde{\nu}) = \sigma_{01,\infty}(\tilde{\nu}) - \sigma_{01}(\tilde{\nu})$ multiplied by a factor of 75, and solid curve: linear FTIR-spectrum of the molecule in CDCl$_3$ solution.

Furthermore, the absorptive component is much smaller than the bleaching component which can be explained by a reduction of the transition dipole moment upon network disruption. This is completely in line with the observation of a smaller linear absorption cross section of the *all-anti* tetrol as compared to the *all-syn* diastereomer (*cf.* Fig. 7). In other words, the state $|0_{nb}\rangle$ in Fig. 12 gains spectroscopic character from the *all-anti* compound at the expense of its *all-syn* parent species.

To differentiate whether or not the excess vibrational energy of the state, $|0_{nb}\rangle$, is canonically distributed over the vibrational modes of the molecule, its difference absorption cross section, $\Delta\sigma_{nb}$, is compared in Fig. 14 to representative thermal difference spectra, $\Delta\sigma(\Delta T)$, of the tetrol recorded for various temperature jumps. It should be emphasized that the spectral position of the bleaching component to $\Delta\sigma(\Delta T)$ is rather insensitive to the temperature jump, ΔT. In contrast, the spectral position of the zero crossing feature separating induced bleach from induced absorption slightly shifts to higher frequencies with increasing ΔT. The overall magnitude of the bleaching component scales linearly with ΔT corresponding to a decreasing OH-stretching transition dipole with increasing temperature. This in turn can be explained by anharmonic coupling of the OH-stretching vibration to low-frequency modes of the hydrocarbon backbone whose higher lying vibrational states become increasingly populated upon thermal excitation. The characteristic absorptive feature on the blue side of the stationary absorption spectrum is due to a thermally induced weakening of the hydrogen-bond network.
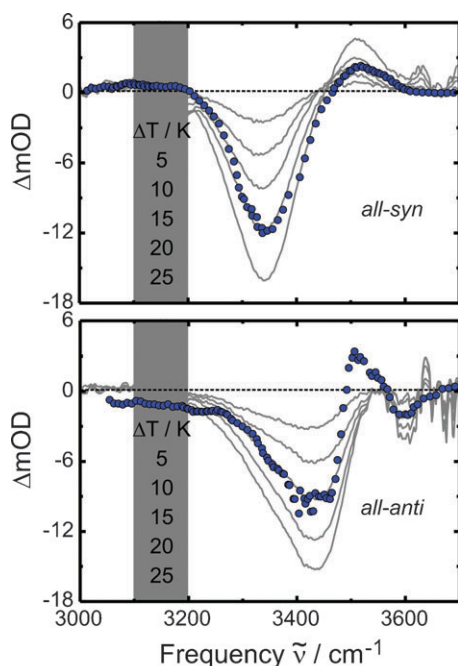

Fig. 14 Top: comparison of thermal difference spectra (gray curves) for various temperature differences with the difference cross section $\Delta\sigma_{nb}$ (blue symbols) of the *all-syn* tetrol multiplied by a factor of four. Bottom: comparison of thermal difference spectra (gray curves) for various temperature differences with a transient absorption spectrum of the *all-anti* tetrol recorded at a pump–probe time delay of 10 ps multiplied by a factor of 40.

Obviously, the state, $|0_{nb}\rangle$, is characterized by a difference absorption cross section, $\Delta\sigma_{nb}$, which closely resembles a thermal difference spectrum of the tetrol. Hence, we can take the qualitative agreement as evidence that the excess energy following hydrogen-bond breakage is canonically distributed over the vibrational degrees of freedom. Within the accuracy of the data, the state $|0_{nb}\rangle$ can be regarded as the "hot" molecule.

That hydrogen-bond breakage following OH-stretching excitation must occur in the *all-syn* species becomes clear when we compare its mid-IR response with that of the *all-anti* compound. Whereas the *all-syn* compound exhibited biexponential kinetics the time-resolved traces of the *all-anti* were purely single-exponential in character. The second slower component was assigned to hydrogen-bond re-association occurring with a time constant of 14 ps. This component is clearly absent in the *all-anti* diastereomer. There, only a long-time constant offset spectrum can be deduced which is compared in Fig. 14 to representative thermal difference spectra.

In contrast to the *all-syn* counterpart, the thermal difference spectra of the *all-anti* species do not exhibit a blue-shifted induced absorption characteristic for a weakened hydrogen-bond network. This finding can be explained by the Langevin simulations described above. These calculations have shown that small-scale fluctuations of the H-bond lengths due to local bending and stretching motions are equally fast for both diastereomers. On the other hand, the two diastereomeric forms differ in the time scales of the large amplitude motions related to full H-bond-breakage and formation. A heating of the *all-syn* species will certainly accelerate the equilibrium H-bond dynamics and therefore, increase the contributions of disrupted network configurations to the OH-stretching absorption cross section—hence, a thermally induced and blue-shifted absorption can be detected for this compound.

For the *all-anti* tetrol, this thermal effect cannot be so pronounced because already at room temperature, H-bond breakage and formation are so fast that all geometrically possible hydrogen-bond lengths become accessible to the molecules (see Fig. 6). In other words, hydrogen-bonded and non-bonded configurations contribute equally to the absorption spectrum of the *all-anti* OH-stretching resonance even at temperatures as low as 300 K. Neither a stationary nor a transient heating of the *all-anti* tetrol (*e.g.* such as that caused by mid-IR excitation) will be able to further shift the structural equilibria in the direction of disrupted networks because the hydroxyls are able to fully sample their entire configuration space and all network configurations are equally populated even before a heating is externally imposed. Consequently, the thermal difference spectrum of the *all-anti* tetrol will not display a blue-shifted absorption typical for a weakened H-bond network as is the case for the *all-syn* diastereomer. The only heating effect on the absorption cross section of the *all-anti* tetrol is an overall increase of the bleaching component that scales linearly with the temperature jump. As mentioned above, this is caused by thermal excitation of the low-frequency backbone modes which anharmonically couple to the OH-stretching transition dipole.

This journal is © the Owner Societies 2009

Phys. Chem. Chem. Phys., 2009, **11**, 8484–8495 | 8493

Within the signal-to-noise ratio, one can assign the long-time transient spectrum of the *all-anti* tetrol to the "hot" molecule. The small induced absorption feature in the pump–probe spectrum at 3500 cm^{-1} originates most likely from the excited stretching state of the dangling hydroxyl group with which the pump-laser had significant spectral overlap. A pump–probe transient recorded at a frequency of $\sim$3600 cm^{-1} (see Fig. 11) reveals indeed an OH-stretching lifetime of 9 ps for the dangling OH, which is long enough for its transient absorption to show up in the 10 ps pump–probe spectrum of Fig. 14. Note, that this lifetime of the "free" OH-stretch is also in quantitative agreement with that of monomeric ethanol molecules in carbon tetrachloride solution.[55]

The offset (*i.e.* long-time) transient spectrum indicative of the existence of the "hot" molecule implies that vibrational energy transfer from the *all-anti* tetrol to the non-polar solvent is simply too slow to be discernible from the data with its limiting delay range of 12 ps only, hence, single-exponential kinetics are observed. Furthermore, it also demonstrates that hydrogen-bond re-association facilitates and accelerates the energy dissipation and provides evidence that mid-IR induced hydrogen-bond breakage must occur in the *all-syn* tetrol.

We also performed preliminary experiments on the *all-anti* tetrol with pump-pulses tuned to the red edge of the linear absorption spectrum thereby trying to excite only those molecules that are engaged in strong hydrogen-bonds. In this case, we did indeed observe a second kinetic component with a small amplitude whose time constant was 20 ps and which may be ascribed to "cooling". Experiments related to the full pump wavelength dependence are still ongoing.

The singular time constant of 1.3 ps obtained by the global fitting procedure of the *all-anti* data is likely to quantify the dynamics of pure intramolecular energy redistribution. This is because energy transfer to the non-polar solvent can be expected to be as slow as the monomeric lower alcohols reported previously. The vibrational structure derived by the DFT calculation suggests a number of different intramolecular pathways for the *all-anti* tetrol. It may be possible that the initial OH-stretching quantum decays into the first overtone of the OH-bending modes. These in turn can then resonantly and hence, rapidly partition into CH-bending and low-frequency CC-backbone modes. Alternatively, the OH-stretching state may decay directly into the CH-stretching manifold while the energy mismatch is compensated for by excitation of low-frequency (*i.e.* $\sim$500 cm^{-1}) backbone modes.

V.   Conclusions

In summary, we have introduced the hydrogen-bonded networks of stereo-selectively synthesized poly-alcohols as low-dimensional model systems for the vibrational dynamics and the vibrational spectroscopy of random hydrogen-bonded networks typically encountered in nature. Depending upon the stereochemical orientation of their hydroxyl groups the poly-alcohols can form collective hydrogen-bonded contacts that are either prototypical for rigid solid-like networks or they are prototypical for highly flexible liquid-like random networks. Quantum chemical calculations demonstrate that the OH-stretching vibrational modes are fully delocalized over

the hydrogen-bond wire when the stereochemical orientation favors the formation of a rigid network (*all-syn*). In contrast, the OH-stretching vibrations become more localized in nature when the network formation is strongly inhibited by stereochemical constraints (*all-anti*). Langevin molecular dynamics simulations were employed to further elucidate the equilibrium dynamics related to hydrogen-bond breakage and formation in the diastereomeric tetrols dissolved in room temperature liquids. Finally, femtosecond mid-infrared spectroscopy was used to explore the ultrafast dynamics related to vibrational energy relaxation in these systems following an initial OH-stretching excitation. In the rigid networks (*all-syn*) vibrational relaxation is dominated by intramolecular energy redistribution mediated by hydrogen-bond dissociation on a time scale faster than 1 ps. The existence of an intermediate state of thermal character exhibiting a disrupted H-bond network can be derived from the mid-IR pump–probe response. Subsequently, H-bond re-association occurs on a time scale of 15 ps and is accompanied by vibrational energy transfer to the non-polar solvent leading to an effective "cooling" of the network. In the flexible networks (*all-anti*) the pump–probe data reveal only a single relaxation process, which is attributed to IVR with a time constant of 1.3 ps. The subsequent "cooling" of these flexible networks is obviously slower than in the rigid networks and too slow to be detected within our limited scan range. A comparison of the data on the two diastereomers shows that hydrogen-bond breakage and re-formation facilitate and accelerate vibrational energy redistribution as well as cooling.

We are currently in the process of performing femtosecond 2-dimensional IR-spectroscopy as well as IR-photon echo peak shift measurements to determine the time scales of vibrational spectral diffusion and to substantiate the Langevin molecular dynamics simulations presented here. These studies will be supplemented by more realistic non-equilibrium molecular dynamics simulation to directly address the time scale for hydrogen-bond recombination following their initial dissociation.

Acknowledgements

References

1 P. Schuster, G. Zundel and C. Sandorfy, *The Hydrogen Bond: Recent Developments*, North Holland, Amsterdam, 1976.
2 *Hydrogen Bonding-New Insights*, ed. S. J. Grabowski, Springer, Amsterdam, 2006, vol. 3, p. 519.
3 G. C. Pimentel and A. L. McClellan, *The hydrogen bond*, W.H. Freeman, San Francisco, 1960.
4 *The Physics and Physical Chemistry of Water*, ed. F. Franks, Plenum Press, New York, 1972, vol. 1.
5 *Protein-Ligand Interactions*, ed. H.-J. Böhm, G. Schneider, Wiley-VCH, Verlag, 2005.
6 E. T. J. Nibbering and T. Elsaesser, *Chem. Rev.*, 2004, **104**, 1887.

7 M. F. Kropman, H. K. Nienhuys, S. Woutersen and H. J. Bakker, *J. Phys. Chem.*, 2001, **105**, 4622.

8 H. K. Nienhuys, S. Woutersen, R. A. van Santen and H. J. Bakker, *J. Chem. Phys.*, 1999, **111**, 1494.

9 S. Woutersen, U. Emmerich and H. J. Bakker, *Science*, 1997, **278**, 658.

10 K. Winkler, J. Lindner, H. Bürsing and P. Vöhringer, *J. Chem. Phys.*, 2000, **113**, 4674.

11 K. Winkler, J. Lindner and P. Vöhringer, *Phys. Chem. Chem. Phys.*, 2002, **4**, 2144.

12 W. Mikenda, *THEOCHEM*, 1986, **147**, 1.

13 A. Novak, *Struct. Bonding*, 1974, **18**, 177.

14 A. Kandratsenka, D. Schwarzer and P. Vöhringer, *J. Chem. Phys.*, 2008, **128**, 244510.

15 K. B. Møller, R. Rey and J. T. Hynes, *J. Phys. Chem. A*, 2004, **108**, 1275.

16 R. Kumar, J. R. Schmidt and J. L. Skinner, *J. Chem. Phys.*, 2007, **126**, 204107.

17 C. J. Fecko, J. D. Eaves, J. J. Loparo, A. Tokmakoff and P. L. Geissler, *Science*, 2003, **301**, 1698.

18 M. L. Cowan, B. D. Bruner, N. Huse, J. R. Dwyer, B. Chugh, E. T. J. Nibbering, T. Elsaesser and R. J. D. Miller, *Nature*, 2005, **434**, 199.

19 J. J. Loparo, S. T. Roberts and A. Tokmakoff, *J. Chem. Phys.*, 2006, **125**, 194521.

20 J. J. Loparo, S. T. Roberts and A. Tokmakoff, *J. Chem. Phys.*, 2006, **125**, 194522.

21 T. Steinel, J. B. Asbury, S. A. Corcelli, C. P. Lawrence, J. L. Skinner and M. D. Fayer, *Chem. Phys. Lett.*, 2004, **386**, 295.

22 J. B. Asbury, T. Steinel, C. Stromberg, S. A. Corcelli, C. P. Lawrence, J. L. Skinner and M. D. Fayer, *J. Phys. Chem. A*, 2003, **108**, 1107.

23 D. Schwarzer, J. Lindner and P. Vöhringer, *J. Phys. Chem. A*, 2006, **110**, 2858.

24 D. Schwarzer, J. Lindner and P. Vöhringer, *J. Chem. Phys.*, 2005, **123**, 161105.

25 I. Paterson and J. P. Scott, *J. Chem. Soc., Perkin Trans. 1*, 1999, 1003.

26 I. Paterson and J. P. Scott, *Tetrahedron Lett.*, 1997, **38**, 7445.

27 S. Woutersen, U. Emmerichs and H. J. Bakker, *J. Chem. Phys.*, 1997, **107**, 1483.

28 K. J. Gaffney, I. R. Piletic and M. D. Fayer, *J. Phys. Chem. A*, 2002, **106**, 9428.

29 T. Schäfer, D. Schwarzer, J. Lindner and P. Vöhringer, *J. Chem. Phys.*, 2008, **128**, 064502.

30 C. Gennari, S. Ceccarelli, U. Piarulli, K. Aboutayab, M. Donghi and I. Paterson, *Tetrahedron*, 1998, **54**, 14999.

31 I. Paterson and J. P. Scott, *Tetrahedron Lett.*, 1997, **38**, 7441.

32 W. D. Cornell, P. Cieplak, C. I. Bayly, I. R. Gould, K. M. Merz, D. M. Ferguson, D. C. Spellmeyer, T. Fox, J. W. Caldwell and P. A. Kollman, *J. Am. Chem. Soc.*, 1995, **117**, 5179.

33 M. P. Allen and D. J. Tildesley, *Computer Simulations of Liquids*, Clarendon, Oxford, 1987.

34 A. Nishi, Y. Kamei and Y. Oishi, *Bull. Chem. Soc. Jpn.*, 1971, **44**, 2855.

35 J. J. P. Stewart, *J. Comput. Chem.*, 1989, **10**, 209.

36 F. Neese, *J. Am. Chem. Soc.*, 2006, **128**, 10213.

37 F. Neese, *ORCA—an ab initio DFT and semiempirical SCF-MO package*, Version 2.6.00, Bonn University, 2007.

38 F. Neese, *J. Comput. Chem.*, 2003, **24**, 1740.

39 A. D. Becke, *Phys. Rev. A: At., Mol., Opt. Phys.*, 1988, **38**, 3098.

40 J. P. Perdew and W. Yue, *Phys. Rev. B*, 1986, **33**, 8800.

41 A. Schafer, H. Horn and R. Ahlrichs, *J. Chem. Phys.*, 1992, **97**, 2571.

42 K. Eichkorn, O. Treutler, H. Ohm, M. Haser and R. Ahlrichs, *Chem. Phys. Lett.*, 1995, **240**, 283.

43 J. Neugebauer and B. A. Hess, *J. Chem. Phys.*, 2003, **118**, 7215.

44 R. W. Larsen, P. Zielke and M. A. Suhm, *J. Chem. Phys.*, 2007, **126**.

45 D. Cringus, T. l. C. Jansen, M. S. Pshenichnikov and D. A. Wiersma, *J. Chem. Phys.*, 2007, **127**, 084507.

46 D. Cringus, S. Yeremenko, M. S. Pshenichnikov and D. A. Wiersma, *J. Phys. Chem. B*, 2004, **108**, 10376.

47 H. Graener and G. Seifert, *J. Chem. Phys.*, 1993, **98**, 36.

48 G. Seifert and H. Graener, *J. Chem. Phys.*, 2007, **127**, 224505.

49 G. Seifert, T. Patzlaff and H. Graener, *J. Chem. Phys.*, 2006, **125**, 154506.

50 J. Lindner, D. Cringus, M. S. Pshenichnikov and P. Vöhringer, *Chem. Phys.*, 2007, **341**, 326.

51 J. Lindner, P. Vöhringer, M. S. Pshenichnikov, D. Cringus, D. A. Wiersma and M. Mostovoy, *Chem. Phys. Lett.*, 2006, **421**, 329.

52 S. Ashihara, N. Huse, A. Espagne, E. T. J. Nibbering and T. Elsaesser, *J. Phys. Chem. A*, 2007, **111**, 743.

53 E. J. Heilweil, M. P. Casassa, R. R. Cavanagh and J. C. Stephenson, *J. Chem. Phys.*, 1986, **85**, 5004.

54 Z. H. Wang, A. Pakoulev and D. D. Dlott, *Science*, 2002, **296**, 2201.

55 R. Laenen and C. Rauscher, *Chem. Phys. Lett.*, 1997, **274**, 63.

56 A. Staib and J. T. Hynes, *Chem. Phys. Lett.*, 1993, **204**, 197.

This journal is © the Owner Societies 2009

Phys. Chem. Chem. Phys., 2009, **11**, 8484–8495 | 8495